Published in final edited form as:
Biomaterials. 2013 November ; 34(35): 8918–8924. doi:10.1016/j.biomaterials.2013.06.055.

Toward in vivo detection of hydrogen peroxide with ultrasound molecular imaging

Emilia S. Olson[a], **Jahir Orozco**[b], **Zhe Wu**[a], **Christopher D. Malone**[a], **Boemha Yi**[a], **Wei Gao**[b], **Mohammad Eghtedari**[a], **Joseph Wang**[b], and **Robert F. Mattrey**[a,*]

[a]Department of Radiology, University of California, 410 Dickinson St., San Diego, CA 92103, United States

[b]Department of Nanoengineering, University of California, San Diego, United States

Abstract

We present a new class of ultrasound molecular imaging agents that extend upon the design of micromotors that are designed to move through fluids by catalyzing hydrogen peroxide (H_2O_2) and propelling forward by escaping oxygen microbubbles. Micromotor converters require 62 mM of H_2O_2 to move – 1000-fold higher than is expected in vivo. Here, we aim to prove that ultrasound can detect the expelled microbubbles, to determine the minimum H_2O_2 concentration needed for microbubble detection, explore alternate designs to detect the H_2O_2 produced by activated neutrophils and perform preliminary in vivo testing. Oxygen microbubbles were detected by ultrasound at 2.5 mM H_2O_2. Best results were achieved with a 400–500 nm spherical design with alternating surface coatings of catalase and PSS over a silica core. The lowest detection limit of 10–100 μM was achieved when assays were done in plasma. Using this design, we detected the H_2O_2 produced by freshly isolated PMA-activated neutrophils allowing their distinction from naïve neutrophils. Finally, we were also able to show that direct injection of these nanospheres into an abscess in vivo enhanced ultrasound signal only when they contained catalase, and only when injected into an abscess, likely because of the elevated levels of H_2O_2 produced by inflammatory mediators.

Keywords

Ultrasound; Nanotechnology; Hydrogen peroxide; Molecular imaging; Abscess

1. Introduction

Hydrogen peroxide (H_2O_2) is a toxic byproduct of many physiologic reactions. It plays an important role in inflammation [1], cancer [2], diabetes, aging, cardiovascular disease, and intercellular signaling [3,4], with stimulated neutrophils producing a steady concentration of up to 65 μM in ex vivo assays [5]. As a strong oxidizer prone to formation of free radicals, it can cause considerable damage of inflamed or infected tissues [6]. As such, there has been broad interest in a robust strategy for imaging H_2O_2 in vivo not only to recognize tissues with elevated levels [7,8], but also to gain insights into a wide variety of H_2O_2 associated diseases.

*Corresponding author. rmattrey@ucsd.edu (R.F. Mattrey).

Appendix A. Supplementary data

Supplementary data related to this article can be found at http://dx.doi.org/10.1016/j.biomaterials.2013.06.055.

Ultrasound is the most commonly used clinical cross-sectional imaging technique worldwide. It displays images at real-time speeds by detecting echoes reflected from interfaces separating tissues with different acoustic impedances – the greater the difference in impedance the stronger the echo. Microbubble-based ultrasound contrast agents are approved for clinical use in most countries including the US. Unlike other clinical modalities requiring micromolar (MRI) to millimolar (CT) levels of contrast agent, ultrasound can detect a single microbubble [9], because it can interrogate tissues with specialized pulses to elicit and then recognize the specific non-linear oscillations of the 1–5 μm microbubbles to eliminate most background signals (often referred to as non-linear or contrast mode).

Recent advances in self-propelled chemically-powered catalytic micromotors that move through fluids at velocities as high as 10 mm/s [10,11] have made these devices promising tools to address many biomedical challenges [12,13]. Micromotor converters (MMCs) catalyze the breakdown of H_2O_2 as fuel to propel forward by expelling released oxygen as microbubbles. Under the microscope and with sufficient fuel (>62 mM H_2O_2), MMCs move as projectiles followed by trails of micron-sized microbubbles [10,11].

We report here a new class of ultrasound contrast agents that can catalyze endogenous H_2O_2 to release oxygen microbubbles based on MMC technology. The aims of this study were: 1) demonstrate that ultrasound can detect the expelled oxygen microbubbles; 2) determine if microbubble detection by ultrasound is more efficient than microscopy; 3) determine whether optimally designed particles could allow ultrasound to detect in vivo levels of H_2O_2; 4) determine whether this approach could distinguish activated from naïve neutrophils and 5) perform preliminary testing to see whether the optimal particles could detect H_2O_2 produced in vivo in an abscess model of inflammation.

2. Methods

2.1. Manufacture of platinum-PEDOT micromotors

Micromotors were synthesized as previously described [11]. Briefly, the tubular micromotors were prepared using a common template directed electrodeposition protocol. A Cyclopore polycarbonate membrane, containing 2 μm diameter conicalshaped micropores (Catalog No 7060-2511; Whatman, Maidstone, U. K.), was employed as the template. A 75 nm gold film was first sputtered on one side of the porous membrane to serve as working electrode using the Denton Discovery 18. The sputter was performed at room temperature under vacuum of 5×10^{-6} Torr, DC power 200W and flow Ar to 3.1 mT. Rotation speed is 65. Sputter time 90 s. A Pt wire and an Ag/AgCl with 3 M KCl were ultrasounded as counter and reference electrodes, respectively. The membrane was then assembled in a plating cell with an aluminum foil serving as a contact. Poly(3,4-ethylenedioxythiophene) (PEDOT) microtubes were electropolymerized at +0.80 V using a charge of 0.06 C from a plating solution containing 15 mM EDOT, 7.5 mM KNO_3 and 100 mM sodium dodecyl sulfate (SDS); subsequently, the inner Pt tube was deposited galvanostatically at −2 mA for 1800 s from a commercial platinum plating solution (Platinum RTP; Technic Inc, Anaheim, CA). The sputtered gold layer was completely removed by hand polishing with ~3 μm alumina slurry. The membrane was then dissolved in methylene chloride for 10 min to completely release the microtubes. The latter were collected by centrifugation at 6000 rpm for 3 min and washed repeatedly with methylene chloride, followed by ethanol and ultrapure water (18.2 MΩ cm), three times of each, with a 3 min centrifugation following each wash. All microtubes were stored in ultrapure water at room temperature when not in use.

2.2. Manufacture of catalase micromotors

Catalase lined micromotors were synthesized as per [11]. Briefly PEDOT microtubes were electropolymerized at +0.80 V for a charge of 0.06 C from a plating solution containing 15 mM EDOT, 7.5 mM KNO_3 and 100 mM sodium dodecyl sulfate (SDS); subsequently, the inner gold layer is plated at −0.9 V for 1 C from a commercial gold plating solution (Orotemp 24 RTU RACK; Technic Inc.). The inner Au layer from the bilayer microtubes was functionalized with a mixed MUA/MCH monolayer. A solution of 2.5 mM MUA and 7.5 mM MCH was prepared in ethanol. The microtubes were incubated in the solution overnight. After rinsing the tubes with water for 5 min, they were transferred to an Eppendorf vial containing a 200 μl PBS buffer (pH 5.5) solution with the coupling agents 1-Ethyl-3-[3-dimethylaminopropyl] carbodiimide hydrochloride (EDC), N-hydroxylsulfosuccinimide (Sulfo-NHS) at 0.4 M and 0.1 M respectively, and the enzyme catalase (2 mg mL^{-1}). This incubation was carried out 7 h at 37°C and thereafter rinsed with PBS with a pH of 7.4 and SDS 0.05 wt % for 15 min at each step. Finally the micromotors were washed repeatedly by centrifugation at 6000 rpm for 3 min with water for three times to remove extra catalase in solution before testing.

2.3. Manufacture of layer by layer catalase-coated nanosphere converters (NSCs)

1 μl of negatively charged silicon particles (0.51 μm, SS03N, Sigma) was washed twice by centrifugation for 3 min at 8000 rpm, first with B&W&B and subsequently with DI water. Layers of catalase/PSS were added to the particles by alternate incubation in 50 μl 1 mg/mL catalase solution (C3155-50, Sigma Aldrich) diluted daily into 0.05 M PBS, pH 5.0 and a PSS/saline solution (1 mg/mL PSS diluted into 1 mL 0.05 M PBS, pH 5.0, containing 29 mg NaCl). Between incubations, particles were washed with 100 μl DI water by centrifuging at 8000 rpm for 3 min. These steps were repeated as layers desired. Particles were resuspended in either PBS (pH 7, Gibco) or HBSS (Gibco) prior to experiments.

2.4. Determination of NSC catalase activity

Enzyme activity was determined spectrophotometrically based on the decrease in absorbance of hydrogen peroxide at $\lambda = 240$ nm, according to an adapted method from the Sigma Enzymatic Assay of Catalase (Sigma, protocol EC 1.11.1.6). Briefly, 100 μL of particle solution was washed by centrifugation at 8000 rpm for 3 min and resuspended in 27 μl of PBS pH 7.0 before being added to 773 μl of 11 mM H_2O_2 solution prepared in 50 mM PBS. After 10 s shaking the solution was placed in the 800 μl spectrophotometer cuvette and the decrease in absorbance at 240 nm with time was recorded immediately at 20 °C for 2 min. One unit of catalase is defined as decomposing 1 μmol of H_2O_2 per minute at pH 7.0 and 20 °C.

2.5. Scanning electron microscopy

Scanning electron microscopy (SEM) images were obtained with a Phillips XL30 ESEM instrument, using an acceleration potential of 20 kV. Optical images are captured by an inverted optical microscope (Nikon Instrument Inc. Ti-S/L100), coupled with a 20× objective, a Hamamatsu digital camera C11440 using the NIS-Elements AR 3.2 software.

2.6. Determination of NSC concentration

NSCs were diluted 100-fold into PBS, and injected onto a hemocytometer. The number of particles in a 100 μm^3 was counted manually under light microscopy.

2.7. Ultrasound phantom imaging and quantification

NSCs at the indicated concentration were placed into a transfer pipette modified to contain a port that could be pinned to the back of a water bath. 3mL phosphate buffered saline (PBS,

Gibco) +0.04 M sodium hydrate cholate (NaCH, Sigma) was added to the NSCs through the port, and samples were allowed to sit for approximately 5 min. Under ultrasound operating in contrast mode (GE LogiqE9, 6–15 MHz linear transducer, MI<0.20,14 framesper second), the concentration of hydrogen peroxide was increased by factors of ten (eg. 8 μM, 80μM, 800 μM…) delivered in low volume (3μL or 30μL). NSCs were tested side by side with control nanospheres of the same geometry without catalase. Detection limits were obtained on the fly by two independent observers blinded to the identity of the tubes. The detection limit was defined as the first point at which characteristic rising bubbles were observed and was recorded at the time of the experiment. All experiments were performed in triplicate.

Stacks of images were analyzed using Image J. An ovoid region of interest was drawn encapsulating the largest area of the tube possible while excluding obvious imaging artifact from the sides of the tube when present. This region was averaged both pre (3–10 frames) and post (5–20 frames) administration of H_2O_2. Total intensity was defined as the average of the pre frames subtracted from the average of the post frames.

2.8. Neutrophil purification and activation

Two methods were used to isolate neutrophils, each giving similar results.

2.8.1. Ammonium chloride preparation (modified from Ref. [14])—30 mL of rabbit blood was drawn into a heparinized syringe and spun down at 3000 rcf × 15 m. The plasma was removed and frozen. The hematocrit and the buffy coat were incubated in isotonic ammonium chloride buffer (15:1 by volume, 8.32 g/L NH_4Cl, 0.84 g/L $NaHCO_3$) for 15–20 min. The samples were then spun at 300 rcf for 15 min, then rinsed twice with HBSS for 10 min. Cells were counted using a hemocytometer.

2.8.2. Dextran sedimentation preparation (modified from Ref. [14])—30 mL of rabbit blood was drawn and added to an equal amount of 3% solution of dextran-500 diluted into normal saline. This was allowed to incubate at room temperature until the hematocrit had settled (approx 20 m). Plasma was then removed and centrifuged at 250× *g*. To reduce the number of red cells present, neutrophils were bathed in 20 mL of ice cold 0.2% saline for exactly 20 s. 1.6% saline was then added and the cells were spun for 250 rcf × 10 min. This was repeated once. We did not perform a Ficoll gradient due to time considerations, and by Wright stain these preparations were estimated to be about 50% pure, consistent with the literature [14].

Neutrophil activation was accomplished by addition of PMA at 15 ng/mL for 1 h.

2.9. Determination of H_2O_2 content

H_2O_2 concentration was assayed using Amplex Red reagent (Life Sciences) using a protocol supplied by the manufacturer. Samples were diluted by 50× prior to use, and calibration samples were spiked with non-activated neutrophils from the same experiment to control for the spectral properties of lysed red blood cells inevitably present in the mixture.

2.10. Neutrophil imaging and quantification

Two experimenters (EO and BY) were blinded to the identity of the nanospheres (NSCs or control lacking catalase) and the neutrophil preparations. 25 μL (1.3×10^7) or 250 μL (1.3×10^8) nanospheres were placed into each tube along with 800 μL of saline. Neutrophils were added to a concentration of 1×10^6 cells per mL (typically ~100–200 μL). Images were assessed for bubble formation at the time of the experiment by both experimenters, and preliminary results were documented while still blinded.

Stacks of images were processed using Image J. For quantification, an ovoid region of interest was drawn. Region intensity was averaged for up to 20 frames prior to injection. Depending on the experiment, 80–200 frames were skipped to avoid artifactually introduced microbubbles, and then up to 30 frames were collected and again averaged. Frames in which tube movement caused obvious artifact to move into the ROI were eliminated prior to averaging. Intensities of "pre" images were subtracted from intensities of "post" images.

2.11. In vivo abscess model

Four Sprague Dawley rats (Harlan Laboratories) aged 8–10 months were used for this study. All animal experiments were approved by our institutional animal care and use committee. Methicillin sensitive *Staphylococcus aureus* (MSSA) was grown in LB media (Sigma Aldrich) at 37°C until reaching mid-log growth phase as determined by serial OD 600 nm measurements. Bacteria were then pelleted, and resuspended in 400 μL LB. 25 μL of the resuspension (corresponding to 6×10^8 colony forming units (CFU), determined retrospectively by plating dilutions onto agar plates) was injected subcutaneously into the right lateral thigh of each rat. Animal vital signs and abscess formation were monitored for each rat over the subsequent 4 days by visual examination and ultrasound.

2.12. In vivo ultrasound imaging and quantification

When ultrasound detectable abscesses had formed, animals were anesthetized (1% isofluorane in O_2) for nanosphere injections. Ultrasound imaging was performed using the 15L8 S transducer of a Sequoia 512 (Siemens Medical Solutions, Mountain View, CA) operating at 7.0 MHz, MI = 0.18,16 frames/sec using their CPS microbubble specific imaging mode. Ultrasound images acquired in real-time from before and for several minutes after nanosphere injection were digitally recorded. First, control nanospheres (8×10^5 particles suspended in 50 μL PBS) were injected at the abscess margin under ultrasound guidance and the needle withdrawn. 5–10 min later, an equal number of NSCs were injected at the same site using a different needle. Images were then assessed for changes in signal at the injection site under both contrast mode and B-mode ultrasound.

A second set of two rats without abscesses served as an additional control arm. Both control nanospheres and NSCs were injected into normal lateral thigh muscle bilaterally ($n = 4$ total sites) where no elevated levels of H_2O_2 is expected, followed by US imaging as described above.

Recorded ultrasound frames were analyzed using Image J. Four frames taken prior to NSC injection were averaged as the "pre". Eighty frames taken when movements from the injection subsided were averaged as "post". The "pre" images were subtracted from the "post" images for both control and catalase-containing NSCs in each of four animals and significance was assessed using a 2-tailed Wilcoxan rank sum test. This was repeated for control animals not harboring abscesses.

3. Results

3.1. H_2O_2 detection by MMCs in vitro

Tubular MMCs with a platinum coated inner surface (Fig. 1a) reported [10,11] to produce microscopically visible oxygen microbubbles were imaged after exposure to 65.3 mM (0.2% v/v) H_2O_2 (Fig. 1b) to assess the ability of ultrasound to detect the produced microbubbles. Microbubbles were first detected by ultrasound when MMCs were exposed to 2–5 mM H_2O_2 (Fig. 1c). Single microbubbles observed at low H_2O_2 concentrations became trails of microbubbles as the H_2O_2 concentration increased. At the highest concentrations, the now echogenic MMCs were seen traveling in a direction opposite their microbubble trail (Supp.

Video 1). The microbubbles were visible on both standard ultrasound as well as non-linear imaging, a microbubble-only imaging technique that suppresses all linear tissue signals. Best results were obtained when the highest concentration of MMCs (27,000/mL) was exposed to 42.4 mM (0.13% v/v) H_2O_2 (Fig. 1d). The threshold was lowered further (0.8 mM) when the inner surface of the MMC was coated by catalase. However, like their predecessors these motors were dense and settled quickly to the bottom of the container.

Supplementary video related with this article can be found at 10.1016/j.biomaterials.2013.06.055.

3.2. H_2O_2 detection by NSCs in vitro

Since microbubble production is more critical for ultrasound detection than MMC motion, we re-engineered the MMCs to become high efficiency stationary H_2O_2 nanosphere converters (NSCs) by layering concentric shells of catalase and poly(sodium styrene sulfonate) (PSS) over a 400–500 nm silica sphere (Fig. 2a). This compact spherical design theoretically allows for smaller, less dense particles with biodegradeable components that are more suitable for in vivo use. SEM confirmed uniform spherical particle shapes with a diameter of 400–500 nm (Fig. 2b). With each added layer of catalase NSC yield decreased, but catalase activity per particle increased (Supp Fig. 1); however, the H_2O_2 detection threshold was similar with 3 or more layers (Fig. 2c). Importantly, adding an outer layer of PSS did not affect the H_2O_2 detection threshold or the ultrasound video intensity, indicating that H_2O_2 diffusion through PSS is not rate limiting (Supp Fig. 2). Assembling of catalase on the NSC surface was more efficient for microbubble formation than free catalase in solution, since the latter required >5000U/mL to produce detectable microbubbles (Supp. Fig. 3). In addition to geometry, this may be because the catalase on the surface of the NSCs had a much higher effective concentration, irregularities on the PSS surface eased nucleation, and the NSCs themselves acted as nucleation sites upon insonation of the surrounding oxygen saturated fluid. For all geometries, using plasma to suspend the particles instead of the mixture of PBS and sodium cholate decreased the detection threshold by another 10–100-fold, probably due to the presence of lipids and proteins (Fig. 2c and d). The detection threshold could be further decreased by increasing NSC concentration (Supp Fig. 4), leading to a final detection threshold as low as 10 μM at a NSC concentration of 4.3×10^6/mL.

3.3. Detection of activated neutrophils

Using the 3 catalase-layered NSC particles that produced the best results, we tested whether they would allow the detection of H_2O_2 produced by PMA-activated neutrophils in enriched blood fractions (Fig. 3a). Both dextran sedimentation and ammonium chloride preparations were used for neutrophil separation in separate experiments, with similar results. Wright staining confirmed the presence of neutrophils (Fig. 3b), and an Amplex red assay for H_2O_2 confirmed that the neutrophil enriched fractions contained 8–60 μM H_2O_2 (Fig. 3c), consistent with published data [5]. Neutrophils were counted with a hemocytometer and added to the NSCs, or similar control nanospheres without catalase, suspended in saline for a final cell concentration of $1–3 \times 10^6$ cells/mL. Subjective assessment of real-time ultrasound was made at the time of the experiment by two blinded observers when the PMA-activated or naïve neutrophils were added. Microbubbles were observed only when activated neutrophils were added to NSCs in each of three experiments (Fig. 3d). Both 1.3×10^7 and 1.3×10^8 particles/mL yielded ultrasound detectable microbubbles, although more microbubbles were seen at the higher particle count. The quantification of video intensity within a region of interest drawn over the lumen of the container was averaged over 20 frames. The first 100–200 frames after the addition of neutrophils were ignored to eliminate the potential of erroneously introduced microbubbles. Fig. 3e shows a representative

experiment done in triplicate, confirming the subjective assessment. Similar results were observed in each of four other experiments each done in triplicate.

3.4. In vivo imaging of NSCs in an abscess model

Finally, NSCs were tested in an in vivo model of abscess in rats. Abscesses are characterized by the presence of a large number of activated neutrophils that release H_2O_2 as a response to bacterial invasion. Once adequate abscesses had formed, control nanospheres were injected under ultrasound guidance at the abscess margin, followed by injection of NSC's in a similar location several minutes later. Immediately after injection with NSC's, an echogenic focus formed at the injection site that was best seen on the contrast specific imaging technique (Fig. 4a), not present when control nanospheres were injected (Fig. 4b, Wilcoxon rank sum test, $n = 4$, $U = 16$, $p = 0.02$). In contrast, injection of the control nanospheres and NSC's into normal rat thigh muscle resulted in no detectable microbubbles ($n = 4$, $U = 16$, $p = 0.49$, Supp. Fig. 5). This suggests that since signal was seen only when NSCs were injected, signal is due to microbubble production. Further since microbubbles were only detected when NSCs were injected in abscesses suggests that elevated levels of H_2O_2 is required.

4. Discussion

We have demonstrated that oxygen microbubbles generated by H_2O_2 converters are detectable by ultrasound imaging. By incorporating catalase and changing the geometry of micromotors to optimize microbubble production rather than motion, we decreased the H_2O_2 detection limit to pathophysiologic levels. Recently, proof-of-principle has been offered for several detection strategies for reactive oxygen species, both *in vitro* and in vivo, making use of fluorescence, ultrasound and MRI. Perng et al. propose a non specific detection strategy for reactive oxygen species based on the chemical reaction of allylhydrazine with reactive oxygen species to form nitrogen and propylene gas [15]. The allylhydrazine is encapsulated in liposomes for ease of delivery and to aid in nucleation. In another scheme, Prussian Blue nanoparticles were found to have catalase-like activity that causes breakdown of hydrogen peroxide to form oxygen microbubbles similar to ours [16]. Despite the differences in approaches, each of these detection strategies has a detection limit of 10uM, similar to the scheme presented here. Advantages of using catalase over other techniques are that its activity has been well studied, it is relatively specific and its rapid kinetics are well characterized. Naked oxygen microbubbles have a half-life of 2 min [17], and they are more readily detectable using current ultrasound technology than even clinically used microbubbles because they are not encapsulated in a shell that dampens oscillations [18].

Other approaches under preliminary investigation include fluorescence assays sensitive to nM of H_2O_2 that have been used to detect LPS induced peritonitis in mice [7], and detection of C-13 benzoic acid formed from C-13-benzoyl formic acid by C-13 MRI; however, these approaches are less readily translatable to the clinic. In contrast, ultrasound is widely available in hospital and outpatient settings, inexpensive, and cross-sectional with imaging depth up to 20 cm, all of which will ease potential translation.

By changing the geometry to a silica-based sphere with alternating layers of PSS and catalase (NSCs), we detected pathophysiological levels of H_2O_2 *in vitro*, ex vivo from activated neutrophils, and in preliminary in vivo experiments using a bacterial abscess model. NSCs injected at abscess margins where active inflammatory mediators such as neutrophils are expected to release H_2O_2 produced a detectable ultrasound signal. This was done using contrast-mode imaging, which is more specific for microbubbles than conventional B-mode. Our in vivo model involved injecting NSCs directly at the abscess site, which was known *a priori*. A challenge will be modifying the NSCs so that they will

home or accumulate at sites of inflammation or other areas of elevated H_2O_2 after systemic administration. We anticipate that smaller NSCs (30–150 nm in diameter) will accumulate in the interstitial space by enhanced permeability and retention (EPR) more readily than the current 500 nm versions as was previously observed with perfluorocarbon nanoparticles [19,20]. We may also see enhanced microbubble production from the smaller NSCs due to their overall larger aggregate surface area and increased nucleation sites for a given concentration of effective catalase compared to the 500 nm particles.

5. Conclusion

We have developed a technique for detecting the presence of H_2O_2 with ultrasound imaging with sensitivity sufficient to distinguish activated from naïve neutrophils *in vitro* and to produce signal in an in vivo abscess model. Ultrasound detection of formed oxygen microbubbles by MMCs occurred at 25 times lesser H_2O_2 concentration than motion detection by microscopy, expanding their potential utilization. The outer PSS protects the catalase without hindering H_2O_2 and oxygen diffusion, provides a negatively charged surface that should be less toxic, and can be functionalized for targeting. Miniaturizing the described NSCs further could potentially improve tissue distribution. Our next step is to further miniaturize these particles to make them more amenable to systemic administration.

Supplementary Material

Refer to Web version on PubMed Central for supplementary material.

Acknowledgments

T32-EB005970 provided salary support for EO; Beatriu de Pinoìs Fellowship from the Government of Catalonia provided support for J.O;W.G. is a HHMI International Student Research fellow; Study was supported by ICMIC P50 CA128346 and NSF CBET 0853375. We wish to thank Siemens Medical Solutions for providing the Sequoia 512 scanner as an equipment loan. We would also like to thank Allan Cortes, Ashley Pourazary, Christopher Barback and Jacqueline Corbeil for providing technical assistance and for helpful discussion.

References

1. Stone JR. An assessment of proposed mechanisms for sensing hydrogen peroxide in mammalian systems. Arch Biochem Biophys. 2004; 422:119–124. [PubMed: 14759598]
2. Szatrowski TP, Nathan CF. Production of large amounts of hydrogen peroxide by human tumor cells. Cancer Res. 1991; 51:794–798. [PubMed: 1846317]
3. Cai H, Griendling KK, Harrison DG. The vascular NAD(P)H oxidases as therapeutic targets in cardiovascular diseases. Trends Pharmacol Sci. 2003; 24:471–478. [PubMed: 12967772]
4. Gius D, Spitz DR. Redox signaling in cancer biology. Antioxid Redox Signal. 2006; 8:1249–1252. [PubMed: 16910772]
5. Test ST, Weiss SJ. Quantitative and temporal characterization of the extracellular H_2O_2 pool generated by human neutrophils. J Biol Chem. 1984; 259:399–405. [PubMed: 6323407]
6. Schalkwijk J, van den Berg WB, van de Putte LB, Joosten LA. An experimental model for hydrogen peroxide induced tissue damage: effect on cartilage and other articular tissues. Int J Tissue React. 1987; 9:39–43. [PubMed: 3596956]
7. Lee D, Khaja S, Velasquez-Castano JC, Dasari M, Sun C, Petros J, et al. In vivo imaging of hydrogen peroxide with chemiluminescent nanoparticles. Nat Mater. 2007; 6:765–769. [PubMed: 17704780]
8. Lippert AR, Keshari KR, Kurhanewicz J, Chang CJ. A hydrogen peroxide-responsive hyperpolarized 13C MRI contrast agent. J Am Chem Soc. 2011; 133:3776–3779. [PubMed: 21366297]

9. Klibanov AL, Rasche PT, Hughes MS, Wojdyla JK, Galen KP, Wible JH Jr, et al. Detection of individual microbubbles of an ultrasound contrast agent: fundamental and pulse inversion imaging. Acad Radiol. 2002; 9(Suppl. 2):S279–S281. [PubMed: 12188248]
10. Gao W, Sattayasamitsathit S, Orozco J, Wang J. Highly efficient catalytic microengines: template electrosynthesis of polyaniline/platinum microtubes. J Am Chem Soc. 2011; 133:11862–11864. [PubMed: 21749138]
11. Gao W, Sattayasamitsathit S, Uygun A, Pei A, Ponedal A, Wang J. Polymer-based tubular microbots: role of composition and preparation. Nanoscale. 2012; 4:2447–2453. [PubMed: 22374514]
12. Mallouk TE, Sen A. Powering nanorobots. Sci Am. 2009; 300:72–77. [PubMed: 19438052]
13. Wang J. Can man-made nanomachines compete with nature biomotors? ACS Nano. 2009; 3:4–9. [PubMed: 19206241]
14. Eggleton P, Gargan R, Fisher D. Rapid method for the isolation of neutrophils in high yield without the use of dextran or density gradient polymers. J Immunol Methods. 1989; 121:105–113. [PubMed: 2474025]
15. Perng JK, Lee S, Kundu K, Caskey CF, Knight SF, Satir S, et al. Ultrasound imaging of oxidative stress in vivo with chemically-generated gas microbubbles. Ann Biomed Eng. 2012; 40:2059–2068. [PubMed: 22562306]
16. Yang F, Hu S, Zhang Y, Cai X, Huang Y, Wang F, et al. A hydrogen peroxide-responsive O(2) nanogenerator for ultrasound and magnetic-resonance dual modality imaging. Adv Mater. 2012; 24:5205–5211. [PubMed: 22811026]
17. Gaffney FA, Lin JC, Peshock RM, Bush L, Buja LM. Hydrogen peroxide contrast echocardiography. Am J Cardiol. 1983; 52:607–609. [PubMed: 6613886]
18. Hoff L, Sontum PC, Hovem JM. Oscillations of polymeric microbubbles: effect of the encapsulating shell. J Acoust Soc Am. 2000; 107:2272–2280. [PubMed: 10790053]
19. Mattrey RF, Andre M, Campbell J, Mitten R, Multer F, Hackney D, et al. Specific enhancement of intra-abdominal abscesses with perfluoroctylbromide for CT imaging. Invest Radiol. 1984; 19:438–446. [PubMed: 6511250]
20. Mattrey RF, Brown JJ, Shelton RE, Ogino MT, Johnson KK, Mitten RM. Use of perfluorooctylbromide (PFOB) to detect liver abscesses with computed tomography. Safety and efficacy. Invest Radiol. 1991; 26:792–798. [PubMed: 1938289]

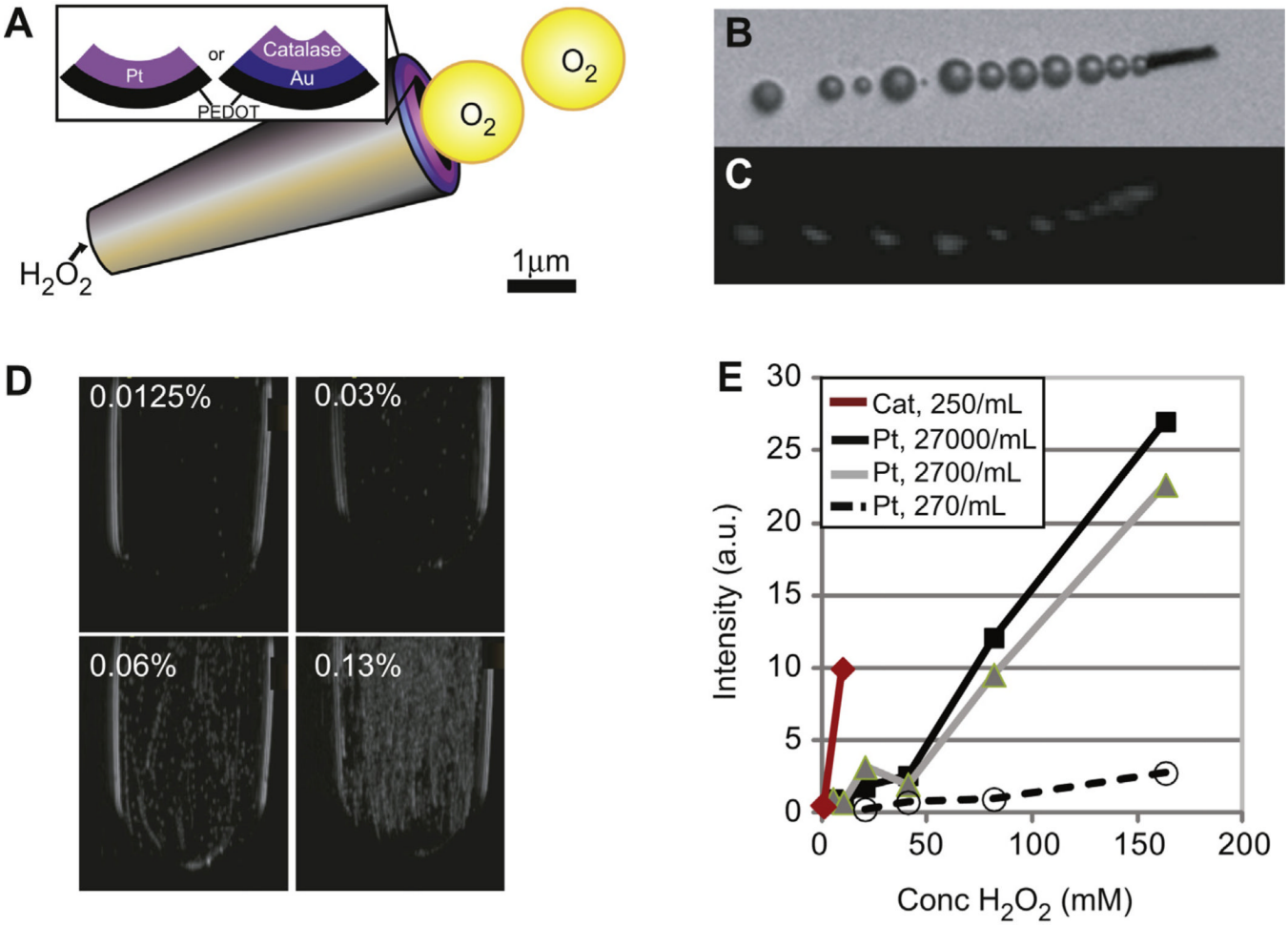

Fig. 1.

Ultrasound based visualization of oxygen microbubbles formed by micromotor converters (MMCs). (A) MMCs are truncated conical structures lined with platinum or catalase over a gold surface, (see inset), acting as catalytic surfaces causing breakdown of H_2O_2 into water and oxygen. (B) Microbubbles can be detected at 0.2% (v/v) (65.3 mM) H_2O_2 using light microscopy. (C) A similar image was generated with ultrasound at much lower H_2O_2 concentration of 0.8 mM. Note that the image in (C) was cropped, rotated and magnified for direct comparison to (B). (D) Microbubble generation as a function of H_2O_2 concentration. Note that few microbubbles are visible at 0.0125% (4.1 mM) produced by few MMCs settled at the bottom. More MMCs become active and the number of microbubbles produced increases with increasing H_2O_2 until a cloud of microbubbles is formed at 0.13% (42.4 mM) H_2O_2. (E) Ovoid regions of interest drawn over the container were used to quantify video intensity in (D), demonstrating a logarithmic relationship between H_2O_2 concentration and ultrasound signal intensity. There is dose dependence on MMC concentration as well as significant improvement when the inner surface is coated with catalase instead of platinum.

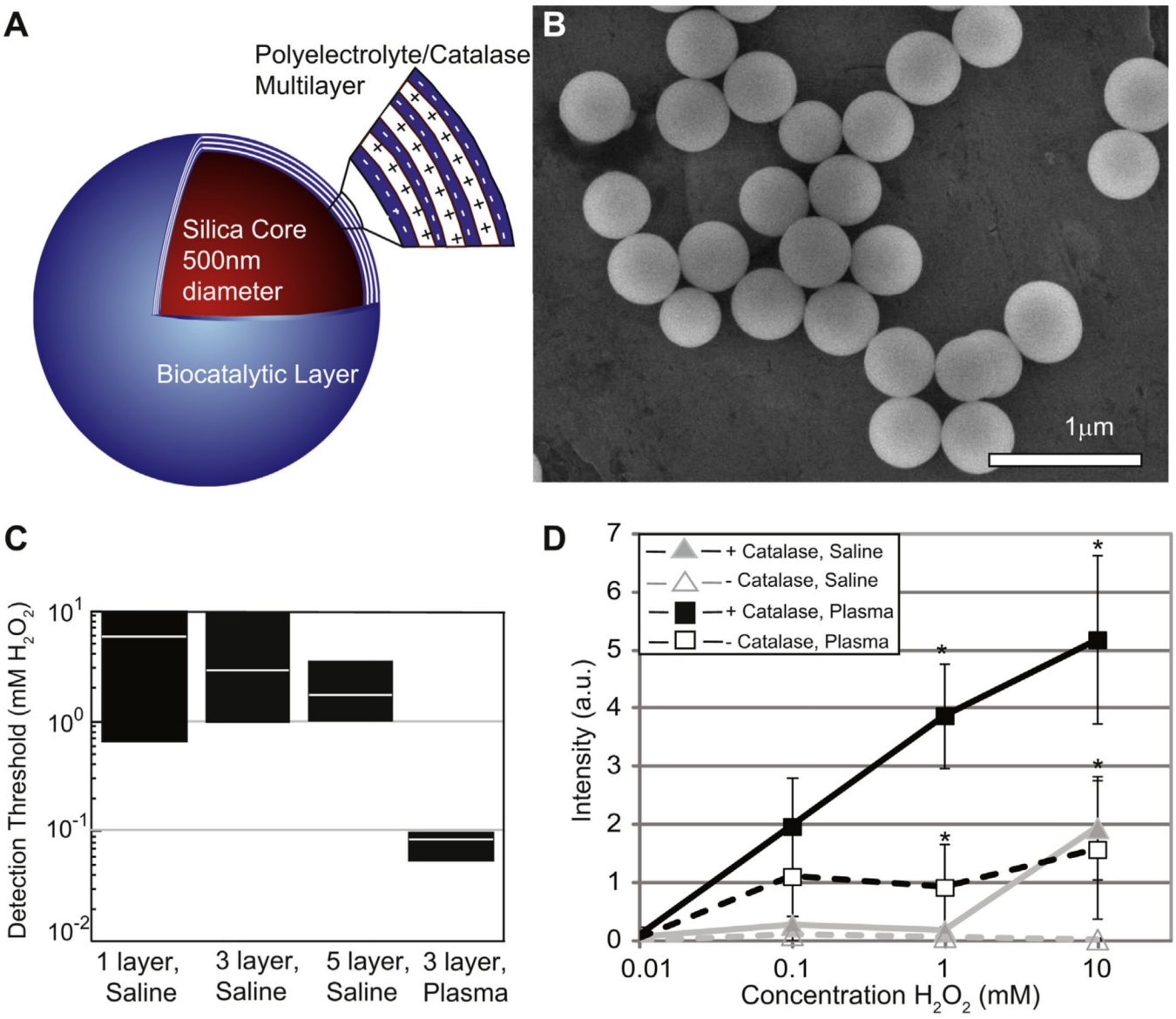

Fig. 2.

Pathophysiologic levels of H_2O_2 are detected by catalase-coated silica nanosphere converters (NSCs). (A) The NSCs contain a 400–500 nm silica core that is coated with alternating layers of negatively charged polyelectrolyte and positively charged catalase (biocatalytic multilayer). (B) Scanning electron microscopy image confirms the spherical shape of the nearly identical 400–500 nm particles. (C) Increasing the number of catalase layers on the outer surface decreases the threshold concentration of H_2O_2 at which microbubbles are first detected by ultrasound with minimal improvement between 3 and 5 layers. The number of NSCs is held constant at 1.3×10^7 (4.3×10^6/mL). Performing the assay in plasma instead of a mixture of buffered saline and sodium hydrate cholate decreases the detection limit by nearly 100 fold to as low as 8 μM. The black rectangles in (C) represent the range of H_2O_2 concentrations at which bubbles are first detected by two blinded observers (n = 6–8). White line within the black rectangles is the average concentration at which bubbles are first detected for each experiment. (D) Video intensity analysis shows a roughly logarithmic dependence of intensity on H_2O_2 concentration when NSCs (squares)

are exposed to increasing amounts of H_2O_2. At each H_2O_2 concentration NSCs produced more microbubbles in plasma (dark rectangles) than in saline, though assays done in plasma have a higher baseline echogenicity than those done in saline. Error bars represent standard error of the mean (n = 3–6). Statistical analysis for comparing NSCs vs. control nanospheres at each data point was performed by 2-tailed unpaired Student's t-test, * indicates $p \leq 0.05$.

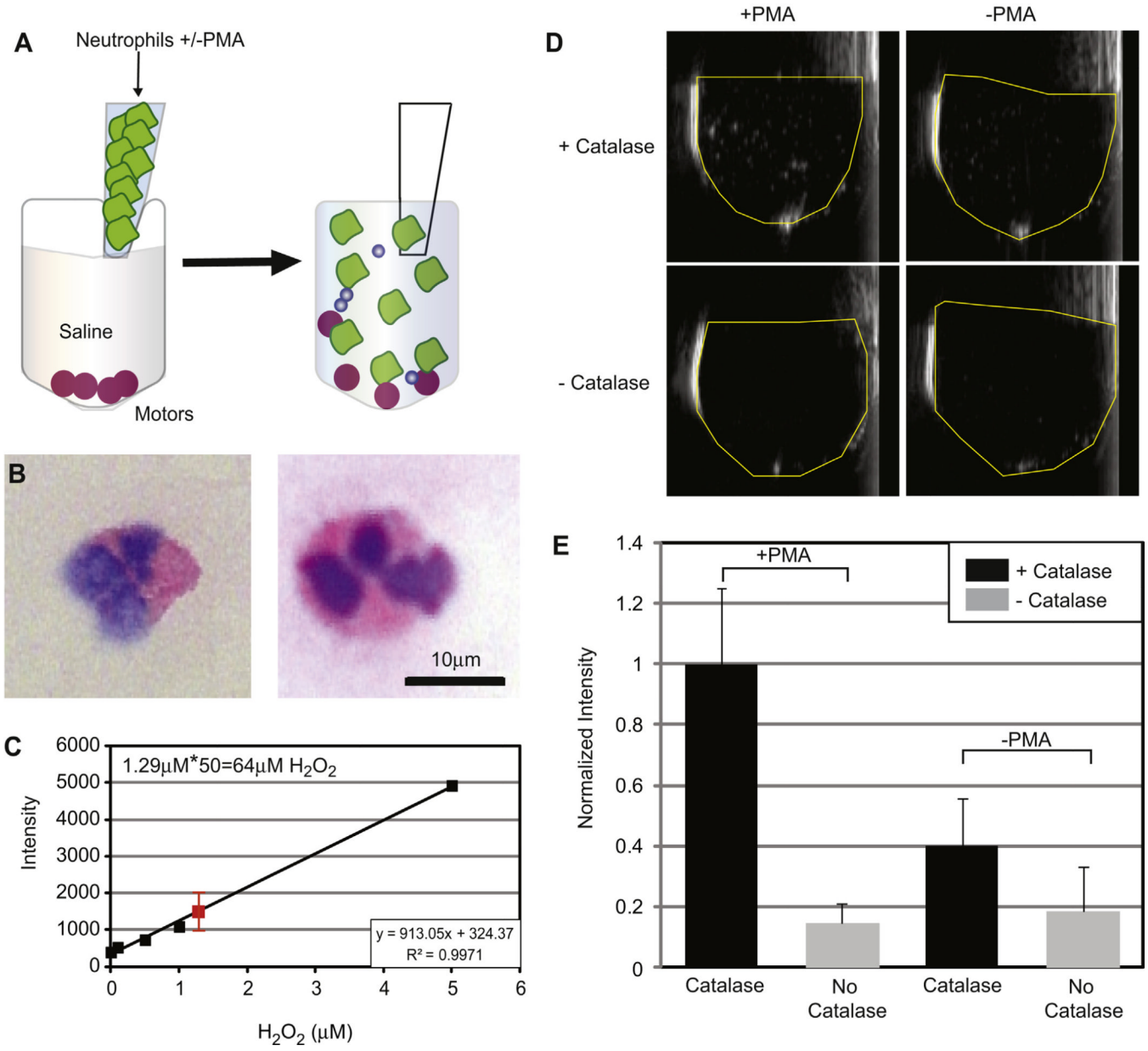

Fig. 3.

Detection of pathophysiologic levels of H_2O_2 by catalase-coated spheres. (A) Neutrophil suspensions (1–3 × 10^6 cells/mL) pre and post PMA activation were added to NSCs and control nanospheres (lacking catalase) suspended in saline using coded containers to blind the observers who rendered judgment whether microbubbles were visible on ultrasound. (B) Exemplary neutrophils after Wright staining. Images were taken at 40×. Preparations contained approximately 50% neutrophils. (C) Scatterplot showing the presence of 64 ± 28 mM H_2O_2 (red square) in the activated neutrophils relative to the non-activated controls by Amplex Red reaction. Unactivated neutrophils were added to the standard solutions to control for the presence of lysed red blood cells in the samples, and samples were diluted 50×. (D) After mixing, microbubbles were only observed in tubes containing activated neutrophils and NSCs. (E) Video intensity analysis of a representative experiment. This experiment was done in triplicate and was normalized to the average value for PMA-treated

neutrophils. Statistical significance was assessed by a 1-way ANOVA ($p = 0.02$). (For interpretation of the references to colour in this figure legend, the reader is referred to the web version of this article.)

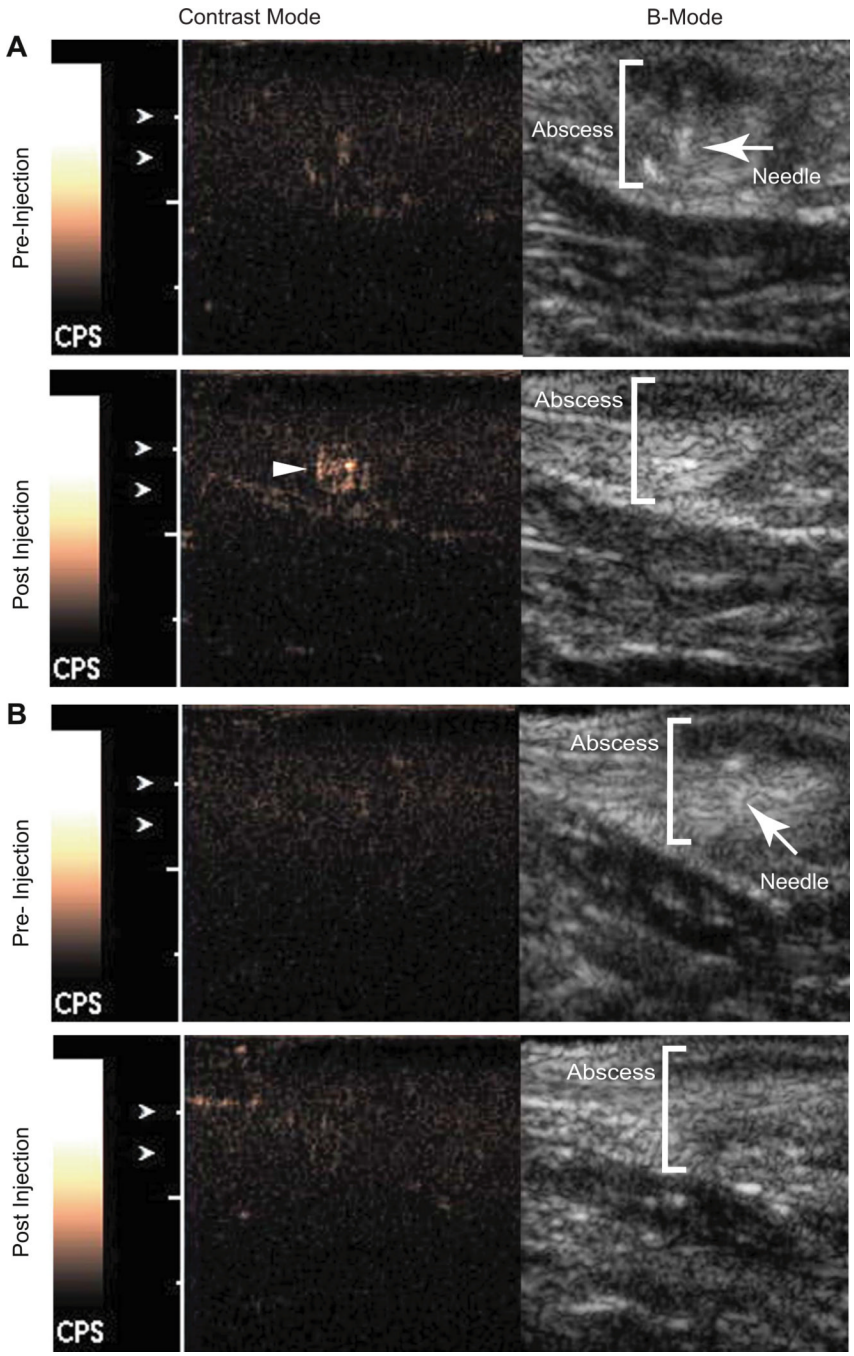

Fig. 4.

NSCs show increase signal in vivo on contrast mode ultrasound when injected at the site of an abscess. (A) NSCs injected at the abscess margin (depicted in orange brackets) results in a discernable increase in signal on contrast mode ultrasound (bottom panel, yellow arrowhead). (B) Control nanospheres of similar geometry but lacking catalase injected in a similar location as in (A) resulted in no appreciable signal (bottom panel). The B-Mode images in top panels of (A) and (B) show the needle (red arrowheads) just before nanosphere injection. The normalized intensity increase resulting from injection of NSCs is significantly greater than that of control nanospheres ($p = 0.02$, $n = 4$). (For interpretation of

the references to colour in this figure legend, the reader is referred to the web version of this article.)